Magnetic behavior of partially filled finite Ising surfaces

Eshel Faraggi,* Linda E. Reichl, and Daniel T. Robb
Prigogine Center for Studies in Statistical Mechanics and Complex Systems, Physics Department, The University of Texas at Austin, Austin, Texas 78712, USA

(Received 21 February 2006; published 11 July 2006)

We study the onset of spontaneous magnetization and the hysteresis properties of finite size two-dimensional Ising spin configurations which are assumed to lie on a smooth nonmagnetic surface. We model the dynamics of the spin system with and without a time-periodic magnetic field using a Monte Carlo simulation. For dilute spin lattices, we find that spontaneous magnetization occurs for spin densities well below thermodynamic predictions; this regime is identified as superparamagnetism. Based on numerical evidence and theoretical arguments we find that for a range of lattice sizes the density is proportional to $\sqrt{T}$ along the line between the paramagnetic regime and the regime in which spontaneous magnetization can occur. We also study hysteresis on four different spin structures for a piece-wise-linear magnetic driving field. We find that the hysteresis loop area depends on the effective exchange coupling as well as the detailed structure of the surface. We define a nearest-neighbor structure constant and study the dependence of the hysteresis loop area on the effective exchange coupling for each of the four different spin structures.

DOI: 10.1103/PhysRevB.74.014407 PACS number(s): 75.70.Ak, 75.40.Gb, 75.60.Ej, 75.30.Kz

I. INTRODUCTION

There is now considerable interest in understanding the magnetic behavior of finite size magnetic dots in thermal contact with their surroundings.[1–3] The magnetic behavior of such systems is not expected to follow thermodynamic predictions since finite size effects will play an important role in determining their behavior. Among the unanswered questions about such systems are the dependence of their structure on the growth mechanism and the dependence of their magnetic properties on their structure.[4,5] Also there is the question of the behavior of small magnetic systems in a time-periodic magnetic field.[6–26] Shen *et al.*[4] find that different deposition processes (thermal and pulsed laser deposition) will result in surfaces with different morphologies and hence different magnetic properties. In addition, there has been significant interest in the behavior of hysteresis loops in thin magnetic films, because seemingly similar experiments can give quite different results as regards the area of hysteresis loops.[16–21]

In this article we focus on the magnetic properties of partially filled finite Ising spin surfaces and the relationship between these properties and the underlying structure. Using the Metropolis algorithm[27,28] we computationally study the onset of spontaneous magnetization in randomly grown, or dilute, surfaces. We then study the relationship between the area of hysteresis loops and the spatial distribution of spins in finite Ising surfaces. In Sec. II we present the tools we will be using. In Sec. III we study the field-free case for randomly deposited Ising systems with different occupation probability. In Sec. IV we study the behavior of hysteresis loop areas for a piece-wise-linear time-periodic driving field. We study four different surface structures: flat, percolating, Sierpinski type fractal, and a numerical representation of a real surface. Finally in Sec. V the results are summarized. We also discuss some auxiliary findings about the Sierpinski fractal in the Appendix .

II. MODEL

Let us consider a two-dimensional rectangular grid which is the substrate on which a surface is grown. We grow various surfaces selecting points on this grid which will be occupied by an Ising spin. The site labeled with i has a spin S_i such that

$$S_i = \begin{cases} 0 & \text{if } i \text{ empty}, \\ \pm 1 & \text{if } i \text{ occupied}. \end{cases} \tag{1}$$

For the case with nearest-neighbor coupling and an applied magnetic field the Hamiltonian is

$$\mathcal{H} = -J\sum_{\langle i,j\rangle} S_i S_j - \sum_{i=1}^{N} S_i H(t), \tag{2}$$

where $\langle i,j\rangle$ denotes nearest neighbor pairs. The magnetic field $H(t)$ is the time dependent driving field, and J is the exchange constant. In the Hamiltonian (2), $\mathcal{H}$, J, and $H(t)$ are chosen to be dimensionless in units of the thermal energy k_BT, with T the temperature and k_B the Boltzmann constant. This choice indicates that only the ratio between the exchange energy (or the total energy in case there are other interactions) and the temperature is relevant. This means that systems with the same configuration, but with different $J_0 = J \cdot k_B T$ (the atomic exchange constant), will behave in the same way at different temperatures. Indeed this behavior is not limited to the Ising model but is exhibited for example in the fact that different ferromagnetic systems undergo a similar phase transition, but at different temperatures.

We would like to have a measure for the structure of the surface so we can relate it to the magnetic properties. We use the average number of nearest-neighbor bonds per spin G,

$$G = N_b/N_p. \tag{3}$$

Here N_b is the number of nearest-neighbor bonds, and N_p is the number of occupied sites. The density of particles $\rho = N_p/N$, where N is the total number of available sites, is equivalent to the occupation probability p for large percolating systems. As we will see, G provides information about

the bond structure of the spin lattice at the minimum length scale.

We restrict our attention here to mature hysteresis loops. By mature hysteresis loops we mean those loops where the two branches of magnetization coincide before the maximal (or minimal) magnetic field value. Note that for a given choice of surface structure and magnetic field profile, we will define a hysteresis loop as the average magnetization curve obtained from an average over many field cycles. Since the area of the hysteresis loop is given by $A=\oint HdM$, where M is the magnetization per spin, A is equal to the magnetic energy per spin dissipated in one loop.

Let us now consider the functional form of the driving field $H(t)$. The usual way of obtaining hysteretic response is to drive the system with a sinusoidal driving field. The area of the loop then depends on two independent parameters, the amplitude of the driving field H_0 and the angular frequency of the driving field $\Omega=2\pi/\tau$, with τ the time period. For sinusoidal driving fields it has been found, at least for frequency ranges containing several orders of magnitude, that the area of the hysteresis loop can have power law behavior of the form $A\propto H_0^{\alpha}\Omega^{\beta}$, where α and β are the power law exponents.[6–9,13–19]

It is possible to restrict the dependence of the hysteretic response to a single parameter $H_0\Omega$ by driving the system with a sawtooth (piece-wise-linear) magnetic field $H(k\tau+t)=H_0\left(2\left|\frac{2t}{\tau}-1\right|-1\right)$, with $0\leq t\leq\tau$, and $k=0,1,2,\ldots$. For the sawtooth field, in the regime of mature hysteresis, the response of the system depends only on the slope of the linear part of the driving field. Let $h=2H_0\Omega/\pi$ denote the absolute value of the slope of the sawtooth driving magnetic field. To see that the hysteresis loop area depends only on this quantity, let $H(t)$ and $H'(t)=H_0'\left(2\left|\frac{2t}{\tau'}-1\right|-1\right)$ be two driving fields, obeying the condition $H_0\Omega=H_0'\Omega'$, and such that the hysteresis loops they produce are mature. Without loss of generality we assume that $H_0<H_0'$. We start with the ferromagnet in the virgin state, with zero magnetization and field. In the regime where both $H(t)$ and$H'(t)$ are less than H_0, the two situations are physically identical. Thus we obtain the same initial magnetization curve for the two fields. If for fields greater than H_0 there is a well defined (unique) magnetization curve, which is the definition for mature hysteresis, then the loops formed will coincide, since for fields between $-H_0$ and H_0 both magnetization curves would have identical starting points and driving fields. As illustrated in Fig. 1, in the regime of mature hysteresis, the contribution to the area of the hysteresis loop will come from the darkened segments of the $H(t)$ versus t curves. Thus for the sawtooth field, in the regime of mature hysteresis, the area of the hysteresis loop depends on the product $H_0\Omega$ in some fashion.

In the following sections, we study the relationship between the structure of a finite Ising spin surface and its magnetic properties. To simulate the dynamics of the systems under consideration, except where otherwise stated, we use the Metropolis algorithm with random updates. We generate pseudorandom numbers using either a linear congruential generator, seeding it with true random numbers obtained in various ways,[27] or by using standard programing functions.

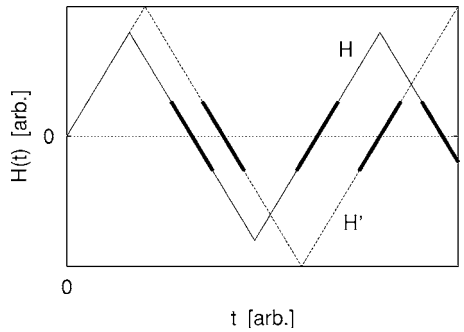

FIG. 1. Two sawtooth driving magnetic fields with the same slope. The thick lines represent the region where the contribution to the hysteresis loop area occurs. Since in both cases the system will start with the same magnetization and will be acted upon by the same field, the hysteresis loop will be the same. Note, however, that under the faster oscillating field the system will dissipate more energy per unit time, since it will complete more loops in a given time.

III. SPONTANEOUS MAGNETIZATION IN FINITE DILUTE ISING SURFACES

We begin by studying the magnetic properties of surfaces where the spins are randomly located. Such systems are known as dilute ferromagnets. Previous studies have found that for a given occupation probability p, the critical temperature T_p^c for the transition between the paramagnetic and ferromagnetic phases is a fraction of the Curie temperature T_1^c for the fully occupied lattice $p=1$ (Refs. 29–36) of infinite extent. In these studies the condition for the transition between paramagnetism and ferromagnetism is the first appearance of a cluster spanning the entire system, called the percolating cluster. The temperature dependent percolation threshold p_c is taken to be the minimum occupation probability for the phase transition point, since it is the minimum probability where a spanning cluster can form. In this section, we show that for finite size Ising surfaces, spontaneous magnetization appears due to finite size effects for spin densities significantly below the thermodynamic prediction $p_c\approx 0.59$.

A. Observable quantities

The surfaces we study have a random distribution of spins. Different distributions of spin with the same occupation probability p can have different values of the magnetization and other observable quantities. For a lattice with N lattice sites occupied by pN spins, the number of possible configurations is $\binom{N}{pN}$. Numerically we find that in most cases averaging over seven pseudorandom realizations produces an average value, of the desired quantity, that differs by less than five percent from the average taken over twenty realizations.

In Fig. 2, we show the average absolute value of the magnetization per spin m for a 40×40 lattice as a function of the spin density ρ. The temperature is fixed at a value $T=0.13T_1^c$, where T_1^c is the critical temperature of the fully occupied $(p=1)$ infinite Ising lattice. We start the surface

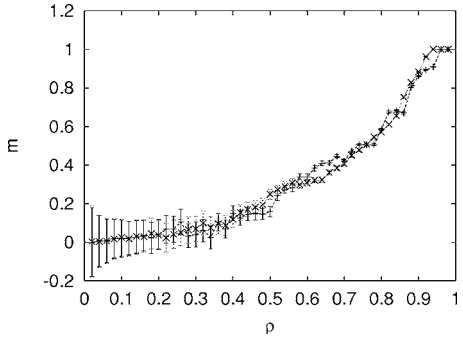

FIG. 2. Absolute value of the average spontaneous magnetization per spin as a function of density for randomly deposited surfaces with $T/T_1^c=0.13$. The two lines correspond to taking an average over seven and twenty realizations of the surface. The smoother curve corresponds to an average over twenty realizations. Bars give the average of the standard deviations in the sampled data.

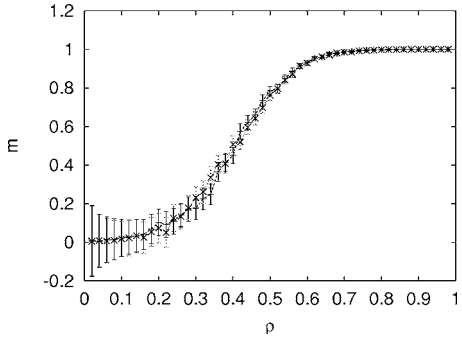

FIG. 3. Spontaneous magnetization per spin as a function of density for seven randomly deposited surfaces with $T/T_1^c=0.13$. A strong field is applied to the system for 10^5 MCSS, the system is allowed to relax without a field for 10^5 MCSS, and measured for 5×10^4 MCSS. The two lines correspond to the field cases $H=1.0(\times)$ and $H=0.5$ (+).

with 32 spins randomly positioned and oriented randomly. We evolve the spins for 25×10^4 Monte Carlo steps per spin (MCSS) and take data for 5×10^4 MCSS. Then 32 spins are added at random locations with random orientation and the system is restabilized and remeasured, etc., until $\rho=0.98$. We repeat this process for several realizations of spin configuration and average the standard deviations and the absolute value of the magnetization obtained for each realization. The two lines in Fig. 2 correspond to an average taken over seven and twenty realizations. The error bars give the average over the standard deviations of the magnetization for the individual runs. As can be seen from Fig. 2, for densities less then $\rho<0.35$, the average magnetization per spin is statistically zero. For larger values of ρ, the average magnetization begins to deviate significantly from zero, but does not increase rapidly until $\rho\approx0.8$, where the increase in the magnetization towards the saturation value occurs more rapidly.

For these low values of spin density where a spontaneous magnetization appears, the surface consists of isolated islands of spin. Each of these isolated islands acts as a separate collection of spins, and undergoes a transition from a disordered state to a ordered state as more and more spins are added to it. The reason that the magnetization due to these isolated islands does not cancel out is because the distribution of islands is not uniform. The largest relevant island controls the net magnetization.

Since we expect that the island distribution would become more uniform as the system size is increased, we can expect that for the infinite system there would be no controlling cluster below the percolation threshold and hence no spontaneous magnetization for the procedure described in the previous paragraph. One should note that if an external magnetic field is applied to the system, either as a seeding field or in hysteresis, the external field will define a preferred orientation and the response would be typical of ferromagnetism, e.g., metastability. To preselect the positive state we also perform the previously described simulation for a 40×40 sample but adding spins with positive orientation, and applying a strong positive field to the system before equilibration and measurements. The system is equilibrated and measured as before without an external magnetic field. Results for this simulation are given in Fig. 3 for the field cases $H=1.0$, 0.5.

In Fig. 4, we give the average energy per lattice site, $\langle\mathcal{H}\rangle/N$ as a function of ρ, for the simulations presented in Figs. 2 and 3. Since the MC method evolves the system according to the thermal distribution, we obtain the thermal average by taking the time average. Figures 2–4 can be understood by considering that Eq. (2) is a measure of the local bonding in the system. In the case of spontaneous magnetization, below p_c each isolated island on the lattice can be in either one of two orientations, and thus generally no global order can form. However, since the energy depends only on the relative orientation of the spins, $\langle\mathcal{H}\rangle$ is independent of the direction of magnetization of a given island. From the viewpoint of energy, where order is represented by alignment of spins and a lower potential energy, order can effectively cover the whole system even for densities less than p_c.

For ferromagnets, hysteresis forms for driving magnetic fields with time periods considerably larger than the relaxation times under sudden field reversal. This is due to the metastability of the system. A dilute surface with occupation probability below p_c is composed of isolated islands of spins. Each of these islands presents a local free energy minimum creating the required metastability. Unlike the global metastability for connected systems where the global transition is smooth, this metastability is composed of a series of meta-

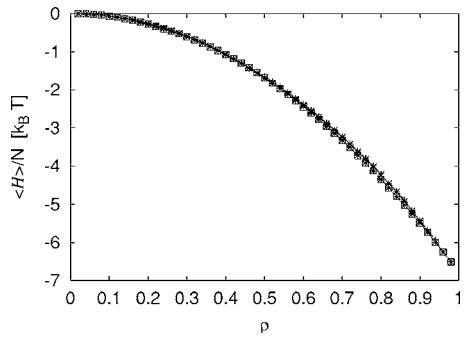

FIG. 4. The average Ising energy $\langle\mathcal{H}\rangle/N$ as a function of density for the systems presented in Figs. 2 and 3. The bars give the average of the standard deviations for each realization.

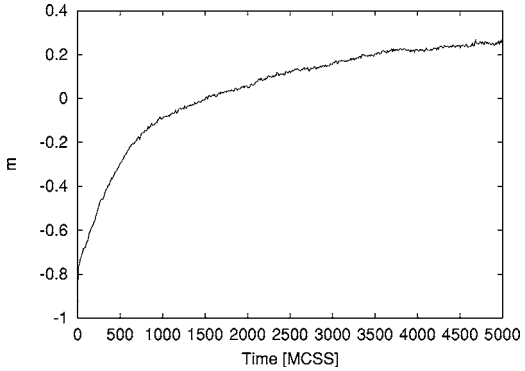

FIG. 5. Relaxation of the magnetization for a 100×100 Ising surface with density 0.4 and $T/T_1^c=0.1$ acted on by a constant field $H=1.0$. The half reversal time of this system is estimated to be 1500 MCSS.

stable wells. This can be observed in the hysteresis loops. In Fig. 5 we plot the magnetization curve of a 100×100 system with $\rho=0.4$ and $T=0.1T_1^c$. The system is prepared in the down orientation and acted on by a constant magnetic field $H=1.0$. The time for reversal of half of the spins is estimated to be about 1500 MCSS. In Fig. 6 we give the hysteresis loop produced by a sawtooth field with $H_0=4.0$ and a time period of 10^5 MCSS, significantly above the half reversal time for the same temperature and density. We see that below the percolation threshold there is enough local order to support metastability in the system.

Two quantities which typically have special behavior near the critical point of a thermodynamic system, are the susceptibility and heat capacity. For dilute systems some remnants of the thermodynamic behavior of the fully occupied system remains, but also significant differences occur. These differences have been studied for the case of $\rho\geq0.6$.[31,32,37] In these studies it was found that the susceptibility has a peak at the critical temperature for a given density, but the heat capacity goes through a maximum at a higher temperature.[38] As part of the preparation for this work we have repeated these studies and found similar results. We have also studied the behavior of the susceptibility and heat capacity for values of $\rho<0.6$ and find similar behavior. In Fig. 7 we show these

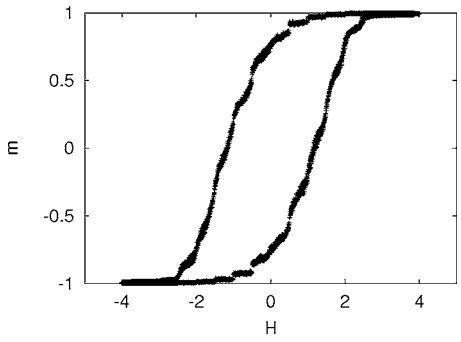

FIG. 6. Hysteresis loop for the 100×100 Ising surface with density 0.4 and $T/T_1^c=0.1$. The driving magnetic field is taken with amplitude $H=H_0/k_BT=4.0$ and time period 10^5 MCSS. The individual metastable states can be observed in this global hysteresis curve.

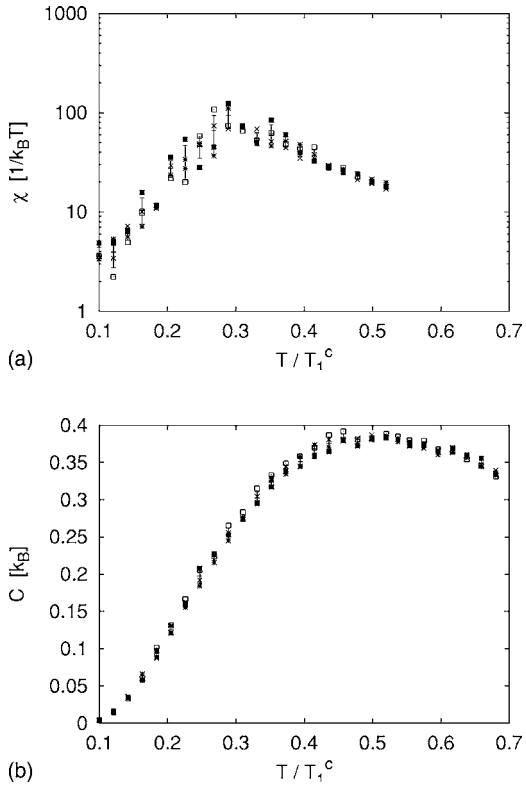

FIG. 7. (a) Susceptibility versus temperature on a semilog plot and (b) heat capacity versus temperature obtained from the Metropolis algorithm on a 100×100 lattice with $\rho=0.5$. The different points correspond to different seeds in the random number generator. Error bars give the standard deviation of the distribution of points resulting from the different seeds.

quantities for $\rho=0.5$, below the percolation threshold.

The susceptibility and the heat capacity were obtained in Fig. 7 using the Metropolis algorithm.[39] The systems are typically evolved from the random state for 10^5 MCSS at the highest temperature for the plot. Then for each point the system is stabilized for 10^4-10^5 MCSS and data is taken for 2×10^5 MCSS. To obtain a more independent set of observations, measurements were taken at 10–20 MCSS intervals. We find a clear peak in the susceptibility and a broad maximum in the heat capacity at a higher temperature. This different transition behavior results from each island of spins on the surface being composed of smaller clusters of aligned spins connected by few border spins. As explained by Heuer,[31] when such a cluster flips, contribution to the heat capacity results only from the few border spins, while contributions to the susceptibility come from the entire flipping cluster.

B. Regions of spontaneous magnetization for finite lattices

In Fig. 8, we show the regions of nonzero spontaneous magnetization for a dilute 100×100 square Ising lattice, as a function of temperature and density. Below we discuss how this diagram is obtained. Let (ρ,T_p^c) be a point along the line between the regions with zero and nonzero spontaneous magnetization, and let J_p^c be the exchange constant at the

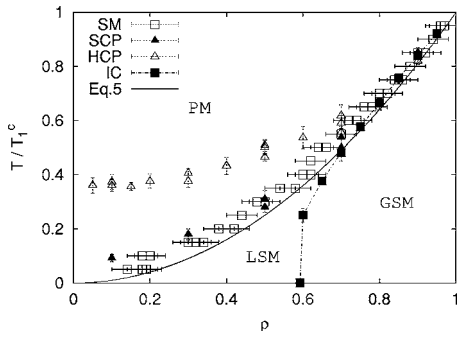

FIG. 8. Regions of zero and nonzero spontaneous magnetization in the density-temperature plane, for 100×100 Ising surfaces, obtained from Monte Carlo simulations using the various conditions described in the text. SM (empty squares) corresponds to the spontaneous magnetization condition, SCP (full triangles) to the maximization of the susceptibility, HCP (empty triangles) to the maximization of the heat capacity, and IC (full squares) corresponds to the invaded cluster algorithm. Three regimes are designated in the figure: (PM) paramagnetism with zero spontaneous magnetization, (LSM) local spontaneous magnetization in a system composed of isolated spin islands, and (GSM) global spontaneous magnetization in a globally connected system. Eq. (5) refers to Eq. (5).

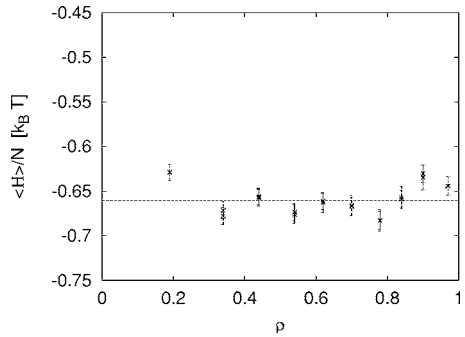

FIG. 9. Average energy $\langle\mathcal{H}\rangle/N$ obtained at the spontaneous magnetization points of Fig. 8. The error bars give the standard deviation of the average energy.

interface between regimes with zero and nonzero spontaneous magnetization. Then, $J_p^c=J_0/k_BT_p^c$, with J_0 the microscopic exchange constant.

The appearance of a nonzero spontaneous magnetization is accompanied by a rapid reduction in the standard deviation δM of the magnetization. As a numerical test for a nonzero spontaneous magnetization in the finite system, we find that the condition $|\frac{\langle M\rangle}{\delta M}|>1$ is useful. Note that for densities below the percolation threshold, since the system is not globally connected, only local order can form. We start our simulation on a $N=100\times100$ rectangular grid with $\rho<0.1$ and the spins in a random state. Since this is a finite system, with an uneven distribution of islands, a method such as the seeding field described above need not be used. The system is cooled to a temperature $T=0.05T_1$ in 10^4 MCSS and the magnetization is calculated for another 10^4 MCSS. We repeat this for 11 more surfaces with the same density, average the absolute value of the magnetization, and average the standard deviation for the different surfaces. The condition $\frac{|\langle M\rangle|_{\text{av}}}{(\delta M)_{\text{av}}}<1$ is checked and, if true, the density is increased by a factor of 1/50. When the condition tests false four times consecutively the density is recorded as the density for the second test, and this density is passed as the initial density for the next temperature, incremented by $0.05T_1$. We take $2\times\frac{1}{50}$ to be the error for the calculation of ρ. This error estimate accounts only for the error in identifying the transition and not for the error from not sampling the entire space of random surfaces. We repeat this for different random seeds in the random number generator to get a better statistical distribution. The estimated limits for the critical densities are shown in Fig. 8 under the heading SM.

In Fig. 9 we plot the average energy per lattice site for the values of density and temperature where the spontaneous magnetization first appears. An interesting property emerges, namely, that $E_c=\langle\mathcal{H}\rangle/N$ is a constant when the spontaneous magnetization first develops. We find that $E_c\approx-0.66$, independent of ρ. This value is consistent with the known critical value of the 2d Ising system $-2J_1^c\tanh(2J_1^c)\approx-0.623$, neglecting the additive term as we do here.[40,41]

Next we define a measure, $\mathcal{S}$, of ferromagnetic bonding for the surface

$$\mathcal{S}\equiv\frac{1}{2}\sum_{i=1}^{N}\sum_{j-n.n}S_iS_j\approx N_b=GN_p, \tag{4}$$

where G is defined in Eq. (3). If all the spins are aligned then the approximation made in Eq. (4) becomes exact. In general one can write $N_b-\mathcal{S}=2\mathcal{L}$, with $\mathcal{L}$ the total length of the border between domains of opposite spin in lattice units, because $S_iS_j=-1$ if i and j are in opposite domains. Thus, this approximation gets better as the domains of aligned spins get bigger. This is approximately the situation near the critical point as the correlation length becomes larger.

We can now obtain a simple analytic estimate for the location of the transition line, in the ρ-T plane, between regions with zero and nonzero spontaneous magnetization. First note that along the line $E_c\approx-J_p^cG_p^cp$, with G_p^c the values of G at the transition for a given occupation probability p. Since for a general percolating surface we have $\langle N_b\rangle=2Np^2$, $G_p^c=2p$, we can write $E_c\approx-2J_p^cp^2$. For the fully occupied surfaces with $G_1^c=2, p=1$ we find $E_c=-2J_1^c$. Equating this with the same expression for a general percolating surface we find that the density at which spontaneous magnetization occurs in the finite size system is given by

$$\rho\approx\sqrt{J_1^c/J_p^c}=\sqrt{T_p^c/T_1^c}. \tag{5}$$

Based on this calculation, the critical density at which spontaneous magnetization occurs is proportional to $\sqrt{T_p^c}$. Within the boundaries of this calculation this result is independent of the spatial dimension D, since $G=pD$ and the dimension would cancel out. Note also that one could relax the assumption that E_c is a constant and allow it to depend on the dimension without changing Eq. (5). The result, Eq. (5), is plotted in Fig. 8 under the heading Eq. (5).

It is interesting that a typical method for locating a thermodynamic phase transition, the invaded cluster algorithm,[42,43] can give misleading results as regards regions

of finite spontaneous magnetization in a finite system. In essence for a given configuration of spins the invaded cluster algorithm tests for the lowest bond probability needed to achieve a globally spanning cluster of aligned spins and performs a step equivalent to a Swendsen-Wang[44] step at that addition probability. As this procedure is repeated it produces a feedback loop that drives the system towards the transition from ferromagnetism to paramagnetism.[27] We use the version of the algorithm which uses a wrap around the periodic boundary conditions as a test for percolation.[43] A main assumption of this algorithm is that the set of occupied sites is globally connected, and hence it would work only for percolating surfaces above p_c. For a given density we perform the invaded cluster algorithm for a dozen deposited surfaces with $L=100$ and average the resulting critical temperature for the transition to the ferromagnetic phase. Our results for this calculation are shown in Fig. 8 under the heading IC. It is useful to note that the agreement for $\rho > p_c$ is quite good between all methods considering that we average over such a small part of the possible surfaces.

Since the regime of local spontaneous magnetization is manifested by isolated clusters of spins we can identify it as a regime of superparamagnetism.[45] In a superparamagnetic system the ferromagnetic particles are gathered in isolated islands of spin, where each island is in the ferromagnetic state but isolated islands do not interact. As proposed by Cowburn[46] the characteristics of superparamagnetism can determine the ultimate density of magnetic random access memory devices.

Finally, we performed a study of the local spontaneous magnetization regime as a function of system size. Before presenting the results it is worth while to note that special care must be exercised when choosing a random number generator for a large simulation where many random numbers are needed. It has been our experience that simple methods for calculating pseudorandom numbers fail for large lattices since the simulation requires more random numbers than the total number of integers available to the compiler. On the other hand we find that standard random packages, e.g., the FORTRAN function RAND, do better in larger simulations. In Fig. 10 we present the points where spontaneous magnetization appears for systems with $L=50$, 71, 100, 141, 200, 283, 400. The lattices are started with random orientations, relaxed for 20 000 MCSS and the magnetization is averaged over 20 000 MCSS. The results for the minimum density where spontaneous magnetization appears are averaged over seven realizations of random surfaces, the bars give the standard deviations for these densities. In the figure Eq. (5) again refers to Eq. (5), reasonable agreement is found between it and the data points for all sizes. The region right of the data points is characterized by local order. As explained previously, such local order can become global if external fields are used even below the percolation threshold, e.g., in hysteresis.

IV. DEPENDENCE OF HYSTERESIS LOOP AREA ON STRUCTURE

In this section, we study the behavior of the area of a hysteresis loop as a function of the slope of a sawtooth magnetic field. With this driving field, for mature hysteresis loops, we have found that the area of the loop depends on a single parameter $H_0\Omega$. We wish to study four distinct structures in two dimensions: a flat plane,[8] a Sierpinski carpet,[47–53] a percolating surface at the percolation threshold,[26] and a numerical representation of a real surface. The real surface was acquired from a printed STM image of a 0.5 monolayer surface.[5] Representations of the fractal, percolating and real surfaces are plotted in Figs. 11–13, respectively.

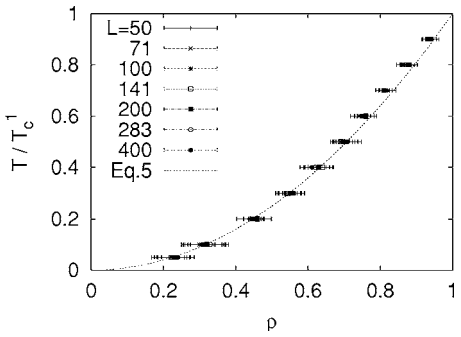

FIG. 10. Regions of spontaneous magnetization for system with $L=50$, 71, 100, 141, 200, 283, 400. For a given temperature, each point in the plot represents the average density where spontaneous magnetization first appears for one of the sizes above. Eq. (5) refers to Eq. (5). Reasonable agreement is found between it and the data points for all sizes.

Before showing results for this system we wish to understand the role of the competing interactions in the Hamiltonian (2), and how they may shed some light on the relation

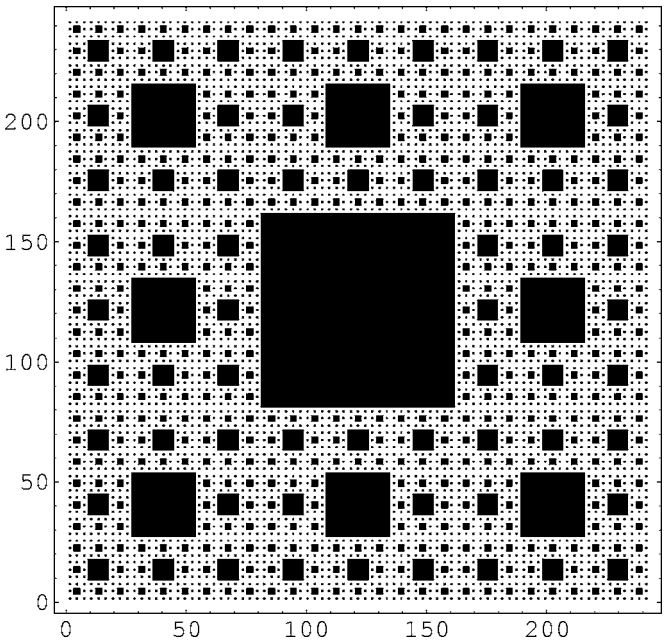

FIG. 11. Sierpinski type fractal approximation generated by the procedure described in the text. The fractal dimension for the completely self-similar fractal is $\frac{\log(8)}{\log(3)}$, $G=1.6$. The number of pairs of nearest neighbors in this $3^5 \times 3^5$ lattice is 52040. Dark regions contain no spins.

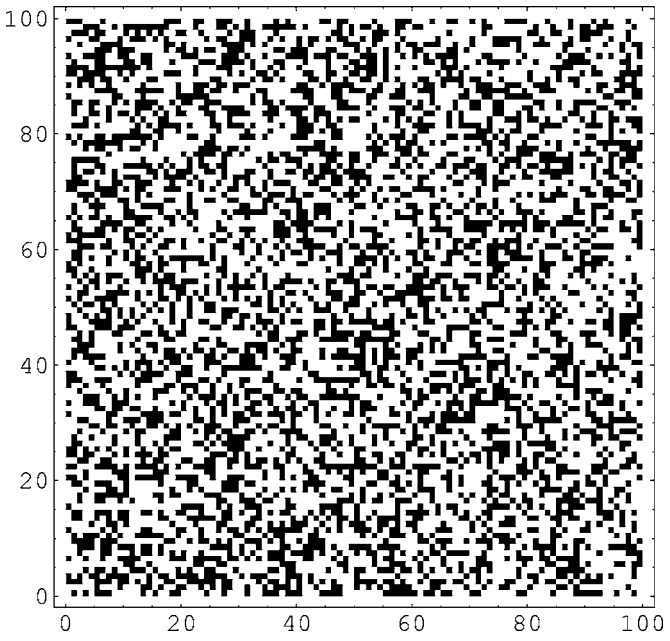

FIG. 12. An example of a percolating surface with occupation probability held close to the percolation threshold $p=0.5927\approx p_c$. Dark regions contain no spins.

between surface structure and the magnetic properties. In the models we use, the exchange interaction is only between nearest neighbors. Thus the exchange energy will depend on the number of nearest neighbors at each site. In Eq. (2) we have two competing interactions; the driving field $H(t)$ and the Ising interaction $J\Sigma_{j-n.n.}S_j$. Since J and $\Sigma_{j-n.n.}S_j$ appear side by side, we can expect the response to depend on each of them in qualitatively the same manner. This means that

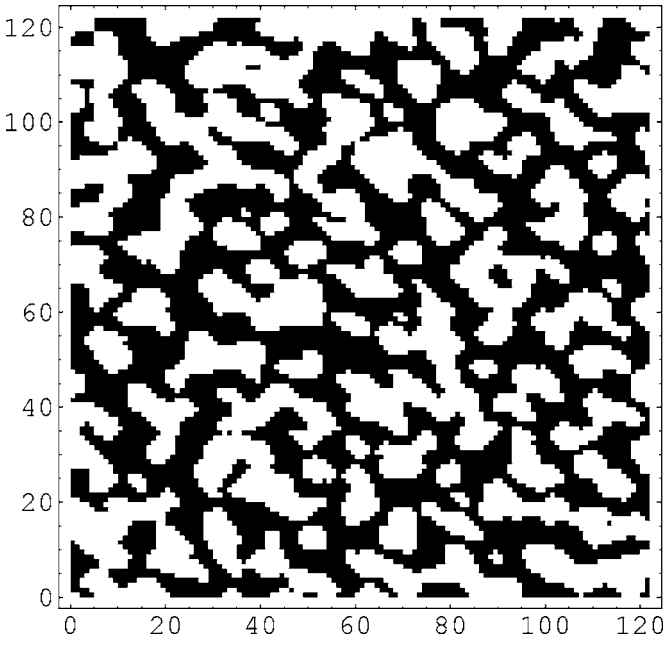

FIG. 13. Numerical representation of an STM image from a 0.5 monolayer Fe surface, deposited on Pd(100) using a thermal deposition process, $G\approx 1.7$. Taken from part of Fig. 2(b) in Jin *et al.* (Ref. 5). Dark regions contain no spins.

increasing the number of nearest neighbors for fixed J will have the same effect on the response to the driving field as increasing J (or lowering the temperature) for a fixed number of nearest neighbors. Since G is a measure of the number of nearest neighbors, we expect changes in magnetic properties resulting from changes in J and changes in G to be correlated.

Our simulations were carried out using the following lattices of Ising spins.

(1) A 100×100 fully occupied lattice with helical boundary conditions ($G=2$),

(2) A 243×243 Sierpinski lattice constructed from the generator,

$$\begin{pmatrix} 1 & 1 & 1 \\ 1 & 0 & 1 \\ 1 & 1 & 1 \end{pmatrix},$$

with zero boundary conditions ($G\approx 1.59$, see the Appendix).

(3) A 200×200 percolating lattice with helical boundary conditions near the percolation threshold $\rho=0.59275$ ($G\approx 1.2$).

(4) A 122×122 lattice graphically acquired from an STM image of a 0.5 monolayer ferromagnetic surface[5] with helical boundary conditions ($G\approx 1.7$).

In helical boundary conditions, sites are labeled consecutively using a one dimensional list. Nearest neighbors to site i in a two-dimensional lattice are $\{i+1,i+L,i-1,i-L\}$, where L is the length of the system, and the last spin is considered neighboring the first spin. In this way the lattice is represented as a toroidal helix. The reason we do not impose helical boundary conditions, or even more standard periodic boundary conditions on the Sierpinski lattice, is that this will change the self similar structure on the largest scale.

The simulation was carried out as follows. Each of the surfaces was started with all the spins having $S_i=1$ and the driving magnetic field at its maximum positive value. The dynamics was then simulated using the Metropolis algorithm of the MC method,[34,35] assuming the energy is given by Eq. (2) with a sawtooth driving magnetic field. For a given exchange coupling we obtain hysteresis loops and their corresponding average area following maturation for several slopes of the driving field. Typical hysteresis loops obtained are given in Fig. 14, and typical area plots are given in Fig. 15. From the area plots we find that a power law dependence of the form $(H_0\Omega)^\alpha$ is valid over the range of parameters of our calculation. The Pearson correlation coefficient[54] between the logarithm of the variables h and A, for example, for the full surface, is 0.998. It is very close to 1, which is the value for a perfect linear relationship. Hence, we calculate power law exponents for the area curves.

Recent work[22–25] suggests that this type of power law behavior of the hysteresis loop is valid only in a finite range of parameter space, with different ranges having different power law exponents. However, in many previous studies, the power law exponents are either computed or measured in the region following maturation of the hysteresis loops, i.e., for $H_0\geq H_c^*$ where, for a given frequency, H_c^* is the first field value where the hysteresis loop matures.[18] In these studies,

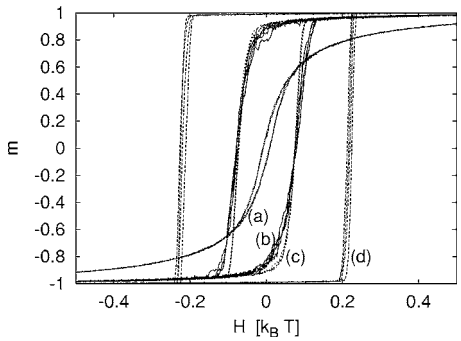

FIG. 14. Typical hysteresis loops obtained for the four different surfaces. Here $J=0.7$, $H_0=1.0$, $\Omega=0.00015$ 1/MCSS. The labels correspond to (a) percolating surface at p_c, (b) real surface, (c) Sierpinski square surface, and (d) fully occupied surface.

as well as our own, for field amplitudes greater than H_c^* mature hysteresis loops have formed and no deviation from power law behavior was found for several orders of magnitude.[6–19,26]

The most condensed surfaces, next to the fully occupied surface, are the Sierpinski and the real surface, having the most neighbors per site. As can be seen from Figs. 14 and 15 these two surfaces respond in a very similar way to a driving field although the distribution of their spins is quite different. The percolating surface has the lowest number of nearest neighbors. Since we see a clear reduction in α as we lower the temperature, we can expect a reduction of the exponents for an increase in G. This is confirmed by the ordering of the exponent for the different surfaces. The reduction of the α exponent for reduced temperatures appears also in the experimental work of Suen and Erskine.[18]

The information about the power law dependence of the area of hysteresis loops for mature hysteresis is summarized in Fig. 16, which gives the hysteresis power law exponents, α, as a function of J for the different structures on a log-log plot. There are several important trends we can identify in Fig. 16. First we notice that α decreases as we decrease the temperature at fixed J_0. For the homogeneous surfaces (full, real, and percolating) we can write this dependence as $\alpha \propto J^{-1}$, and for these surfaces this functional dependence is independent of the surface. The Pearson coefficient between

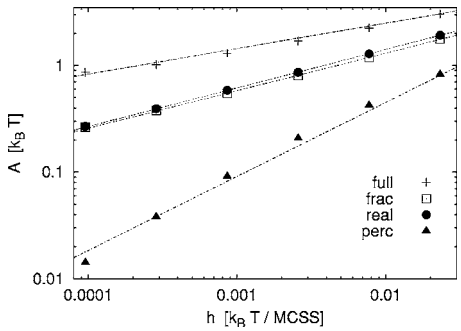

FIG. 15. Log-log plot of the area of the hysteresis loops as a function of the slope of the driving field. Here $J=0.7$. Note how close the behavior of the real and the Sierpinski surfaces is. This is consistent with their close G value.

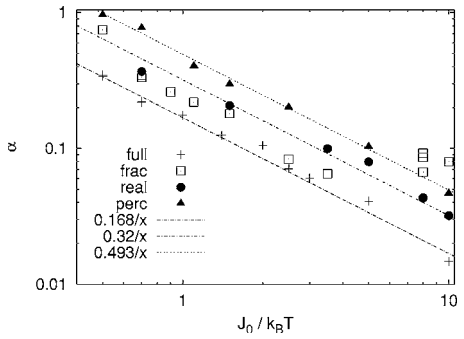

FIG. 16. The power law exponent α as a function of the effective exchange coupling J for the four different surfaces on a log-log scale. We also give the best fit curve for the full, real, and percolating cases.

the logarithm of J and α, for example, for the percolating surface, is 0.997. For the nonhomogeneous Sierpinski surface we find deviations from this dependence for low temperatures. We also find that the structure plays a role in the value of α which is qualitatively similar to the role of J. Surfaces with a higher concentration of nearest neighbors have a lower value of the power law exponent α and vice versa.

We have also performed a study of the dependence of these results on the size of the system for the fully occupied case. Results for lattices of sizes 71^2, 100^2, 141^2, 200^2, 283^2, and 400^2 Ising spins are given in Fig. 17. These results were obtained by using a trivially parallel Monte Carlo program. As is clear from the results, for the range studied the power law exponent are almost independent of the system size.

These trends of the α versus J curve are also qualitatively supported by additional MC studies we have performed on hysteresis loops in percolating systems as a function of the occupation probability and of Sierpinski structures with increasing G.

Finally we note several other studies of magnetization in partially filled Ising surfaces.[26,55,56] Most particularly Zheng

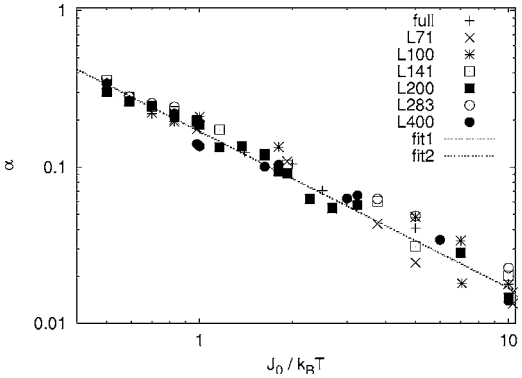

FIG. 17. The power law exponent α as a function of the effective exchange coupling J for square Ising lattices of sizes: 71^2, 100^2, 141^2, 200^2, 283^2, and 400^2. Results from Fig. 16 are given under the label "full". The label "fit1" corresponds to the best fit line given in Fig. 16 for the fully occupied case. The label "fit2" corresponds to a best fit of the data points for the five lattice sizes. The two curves are indistinguishable in the plot.

and Zhang[26] study the scaling of the area of the hysteresis loop in both the percolating and the Sierpinski surface. Trends similar to the ones we report here for the scaling exponent were observed by them for hysteresis in percolating surfaces. For the Sierpinski surface however, they report a constant exponent with a value $\alpha=0.25\pm0.04$ independent of temperature. As presented here, the Sierpinski surface follows the same trends as the other three surface types we study, i.e., the scaling exponent for the Sierpinski surface is temperature dependent. We note that Zheng and Zhang base their conclusion of a constant exponent for the Sierpinski surface on a limited range of exchange coupling, three points at $J=0.5$, 0.6, 0.7. We also note that a α value of approximately 0.3 for $J=0.6$ is consistent with our calculations of the exponent α presented in Fig. 16 for the Sierpinski surface. However, our results indicate that over a broader range of J values the exponent α changes.

V. CONCLUSION

We have studied the relationship between the structure of finite Ising surfaces and their resulting magnetic properties. We have found that for a fixed temperature and number of lattice sites a finite average number of nearest neighbors is needed to achieve nonzero average spontaneous magnetization. We have mapped out regions of nonzero spontaneous magnetization in the (ρ,T) plane for a randomly deposited finite Ising surface and observed nonzero spontaneous magnetization at spin densities smaller than those predicted by thermodynamics. Based on numerical studies and theoretical arguments we find that $T_p^c/T_1^c\approx\rho^2$ along the transition line between zero and non-zero spontaneous magnetization.

For hysteresis loop areas, we have found that the structure of the magnetic surface, effectively measured by G, and the effective exchange coupling play a joint role in determining the power law behavior of the hysteresis loop area for the finite Ising surface. For homogeneous surfaces the dependence of α on J seems to have a universal functional form, independent of the underlying structure $\alpha(J)\propto J^{-1}$, where the structure appears in the proportionality constant. We remark that additional calculations of hysteresis area for partially filled surfaces have been performed,[26,55,56] with the work of Zheng and Zhang[26] the closest to our work. However, our calculations only support their conclusions with regard to power law behavior of hysteresis loop area in percolating surfaces, since in our simulation α is dependent on the temperature for all of the surfaces we studied.

The behavior of α as a function of the exchange coupling is consistent with experiments showing that the distribution of activation volumes becomes more peaked for stronger exchange coupling.[57] A more peaked distribution would mean that the reversal of magnetization in the hysteresis loop would occur along a more narrow strip of magnetic field values. Qualitatively this means that less change in the form of the hysteresis loop (and therefore less change in the hysteresis loop area) is possible as the driving parameters are varied. Thus a lower value of the exponent α is expected for higher J values.

The properties of hysteresis we have discussed for this system may shed light on the differing experimental results on hysteresis power law behavior for seeming similar experiments. Changes in the temperature of the experiment or, more critically, changes in the structure of the deposited surfaces can change the hysteresis area power law exponent. As recent experiments suggest,[4,5] the deposition process can result in different surface structures and, thus, different experiments can produce different power law behavior for the area of the hysteresis loops.

ACKNOWLEDGMENTS

The authors wish to thank the Welch Foundation Grant No. F-1051 and the Engineering Research Program of the Office of Basic Energy Sciences at the U.S. Department of Energy, Grant No. DE-FG03-94ER14465 for partial support of this work. We thank the University of Texas at Austin High Performance Computing Center for their help and the use of their computer facilities. We also thank Natali Teszler for assistance with statistical analysis.

APPENDIX

To construct the Sierpinski-type fractal surfaces considered here, we devised the following method. Our goal is to build a numerical fractal surface, i.e., a finite two-dimensional grid of points S_{mn} (here m and n denote the site position along the x and y axis, respectively). To do this we define a generator matrix for the fractal. For example the generator for the square Sierpinski fractal we have considered earlier is

$$(g_{ij})_{i,j}=\begin{pmatrix}1&1&1\\1&0&1\\1&1&1\end{pmatrix}. \tag{A1}$$

In two dimensions the generator g_{ij} is a square matrix of size $\mathcal{L}\times\mathcal{L}$ with 0/1's representing an empty/occupied generator site. To find whether S_{mn} is occupied or empty we decompose m, n in base $\mathcal{L}$; that is, $m=\Sigma_{k=0}^{\nu-1}a_k\mathcal{L}^k$ and $n=\Sigma_{k=0}^{\nu-1}b_k\mathcal{L}^k$, with a_k, $b_k<\mathcal{L}$. Then,

$$S_{mn}=\prod_{k=0}^{\nu-1}g_{a_kb_k}, \tag{A2}$$

Eq. (A2) is simply a statement that for a given site to be occupied, on all iterations of the fractal the site was part of an occupied block. Here ν can be interpreted as the number of iterations the numerical fractal contains; in a more general sense, $\nu-1$ is the largest power of $\mathcal{L}$ needed in the expansion of the lattice indices. In this way the geometric self-similar structure of the fractal is carried by the self-similar structure of the decomposition in base $\mathcal{L}$. The fractal is obtained in the limit $\nu\to\infty$ under appropriate choice of limit lattices. This construction can be extended to any number of dimensions. Penrose gives a similar but more general discussion, from the perspective of set theory.[58]

The quantity G which we introduced quantifies the nearest-neighbor structure, by definition it is the density of bonds per spin. It is interesting to note that G coincides with

the Euclidean dimension for Euclidean lattices. As an example, a calculation of the quantity G for the infinite square Sierpinski fractal considered earlier is now presented. We create the Sierpinski surfaces starting with a primitive surface with eight occupied sites as in Eq. (A1). At each iteration step ν, eight copies of the previous configuration are created with an additional $8(3^{\nu})$ nearest-neighbor bonds formed between the copies. Hence, we can write $N_{b,\,\nu+1}=8(N_{b,\nu}+3^{\nu})$, with $N_{b,\nu}$ the number of bonds at the beginning of iteration step ν. Since the number of spins at iteration step ν, $N_{p,\nu}=8^{\nu}$, the value of G at step ν can be written as $G_{\nu}=G_{\nu-1}+\left(\frac{3}{8}\right)^{\nu-1}$. Using this last recursion relation, and the initial value $G_1=1$, we find for the infinite square Sierpinski fractal $G=8/5$.

*Electronic address: faraggi@physics.utexas.edu; Present address: Physics Department, Florida International University, Miami, Florida 33199.

[1] W. Wernsdorfer, K. Hasselbach, B. Barbara, L. Thomas, D. Mailly, and G. Suran, J. Magn. Magn. Mater. **145**, 33 (1995).
[2] W. Wernsdorfer, E. B. Orozco, K. Hasselbach, A. Benoit, B. Barbara, N. Demoncy, A. Loiseau, H. Pascard, and D. Mailly, Phys. Rev. Lett. **78**, 1791 (1997).
[3] D. T. Robb, L. E. Reichl, and E. Faraggi, Phys. Rev. E **67**, 056130 (2003).
[4] J. Shen, P. Ohresser, Ch. V. Mohan, M. Klaua, J. Barthel, and J. Kirschner, Phys. Rev. Lett. **80**, 1980 (1998).
[5] X. F. Jin, J. Barthel, J. Shen, S. S. Manoharan, and J. Kirschner, Phys. Rev. B **60**, 11809 (1999).
[6] M. Rao, H. R. Krishnamurthy, and R. Pandit, Phys. Rev. B **42**, 856 (1990).
[7] M. Rao and R. Pandit, Phys. Rev. B **43**, 3373 (1991).
[8] W. S. Lo and R. A. Pelcovits, Phys. Rev. A **42**, 7471 (1990).
[9] S. Sengupta, Y. Marathe, and S. Puri, Phys. Rev. B **45**, 7828 (1992).
[10] F. Zhong, J. X. Zhang, and G. G. Siu, J. Phys.: Condens. Matter **6**, 7785 (1994).
[11] Fan Zhong and Jing-Xiu Zhang, Phys. Rev. Lett. **75**, 2027 (1995).
[12] D. Dhar and P. B. Thomas, J. Phys. A **25**, 4967 (1992).
[13] M. Acharyya and B. K. Chakrabarti, Phys. Rev. B **52**, 6550 (1995).
[14] C. N. Luse and A. Zangwill, Phys. Rev. E **50**, 224 (1994).
[15] A. M. Somoza and R. C. Desai, Phys. Rev. Lett. **70**, 3279 (1993).
[16] Q. Jiang, H.-N. Yang, and G.-C. Wang, Phys. Rev. B **52**, 14911 (1995).
[17] Y.-L. He and G.-C. Wang, Phys. Rev. Lett. **70**, 2336 (1993).
[18] J.-S. Suen and J. L. Erskine, Phys. Rev. Lett. **78**, 3567 (1997).
[19] J.-S. Suen, M. H. Lee, G. Teeter, and J. L. Erskine, Phys. Rev. B **59**, 4249 (1999).
[20] F. Zhong, J. Dong, and D. Y. Xing, Phys. Rev. Lett. **80**, 1118 (1998).
[21] J. L. Erskine and J.-S. Suen, Phys. Rev. Lett. **80**, 1119 (1998).
[22] S. W. Sides, P. A. Rikvold, and M. A. Novotny, J. Appl. Phys. **83**, 6494 (1998).
[23] S. W. Sides, P. A. Rikvold, and M. A. Novotny, Phys. Rev. E **59**, 2710 (1999).
[24] C. Nistor, E. Faraggi, and J. L. Erskine, Phys. Rev. B **72**, 014404 (2005).
[25] E. Faraggi, J. Magn. Magn. Mater. **303**, 49 (2006).
[26] G. P. Zheng and J. X. Zhang, Physica A **264**, 515 (1999).
[27] M. E. J. Newman and G. T. Barkema, *Monte Carlo Methods in Statistical Physics* (Clarendon Press, Oxford, 1999).
[28] N. Metropolis, A. W. Rosenbluty, M. N. Tosenbluty, A. H. Teller, and E. Teller, J. Chem. Phys. **21**, 1087 (1953).
[29] Diertich Stauffer and Amnon Aharony, *Introduction to Percolation Theory* (Taylor and Francis, New York, 1992).
[30] H. Jarzecka and B. Fechner, Physica A **179**, 288 (1991).
[31] H.-O. Heuer, Phys. Rev. B **45**, 5691 (1992).
[32] J.-K. Kim and A. Patrascioiu, Phys. Rev. B **49**, 15764 (1994).
[33] R. Kuhn, Phys. Rev. Lett. **73**, 2268 (1994).
[34] E. S. de Sousa, A. M. Mariz, F. D. Nobre, and U. M. S. Costa, Physica A **241**, 469 (1997).
[35] G. Mazzeo and R. Kuhn, Phys. Rev. E **60**, 3823 (1999).
[36] U. L. Fulco, F. D. Nobre, L. R. de Silva, and L. S. Lucena, Physica A **297**, 131 (2001).
[37] J.-K. Kim and A. Patrascioiu, Phys. Rev. Lett. **72**, 2785 (1994).
[38] For low densities (such that there are isolated free spins), and for low temperatures, the fluctuations of the magnetization will be dominated by the constant flip of those free spins in a Monte Carlo simulation. This means that the fluctuations will remain finite as the temperature goes to zero in the simulation. If one was to calculate the susceptibility from the thermodynamical relation relating the fluctuations to the susceptibility, one would get a diverging susceptibility as the temperature goes to zero since the mentioned relation contains a term inversely proportional to the temperature. As $p \to 1$ the susceptibility converges to zero for low temperatures, which is the basis for us relating this behavior to the free spins. Since the energy is unaware of these isolated spins, the heat capacity converges to zero as the temperature goes to zero.
[39] We find the Wolff algorithm to be faster converging than the Metropolis algorithm. However, for densities below the percolation threshold the Wolff algorithm misses completely the maximization of the susceptibility. This is probably due to a combination of taking the absolute value of the total magnetization in the Wolff algorithm and the fact that when the film is composed of isolated islands the Wolff algorithm flips different islands randomly at criticality while the Metropolis algorithm flips only individual spins, and retains the original island orientation. For this reason we use the Metropolis algorithm, which in general is less suited for problems near the critical point. One should note that both algorithms give identical heat capacity curves.
[40] Linda E. Reichl, *A Modern Course in Statistical Physics*, 2nd ed. (Wiley, New York, 1998), p. 483.
[41] Gregory H. Wannier, *Statistical Physics* (Dover, New York, 1987), p. 339.
[42] J. Machta, Y. S. Choi, A. Lucke, T. Schweizer, and L. V. Chayes, Phys. Rev. Lett. **75**, 2792 (1995).
[43] G. T. Barkema and E. J. Newman, Adv. Chem. Phys. **105** (1999).
[44] R. H. Swendsen and J.-S. Wang, Phys. Rev. Lett. **58**, 86 (1987).

[45] C. P. Bean and J. D. Livingston, Jpn. J. Appl. Phys., Suppl. **30**, 120 (1959).
[46] R. P. Cowburn, J. Appl. Phys. **93**, 9310 (2003).
[47] Y. Gefen, B. B. Mandelbrot, and A. Aharony, Phys. Rev. Lett. **45**, 855 (1980).
[48] Y. Gefen, A. Aharony, and B. B. Mandelbrot, J. Phys. A **16**, 1267 (1983).
[49] Y. Gefen, A. Aharony, Y. Shapir, and B. B. Mandelbrot, J. Phys. A **17**, 435 (1984).
[50] Y. Gefen, A. Aharony, and B. B. Mandelbrot, J. Phys. A **17**, 127 (1984).
[51] G. Bhanot, D. Duke, and R. Salvador, Phys. Lett. **165B**, 355 (1985).
[52] B. Bonnier, Y. Leroyer, and C. Meyers, Phys. Rev. B **37**, 5205 (1988).
[53] B. Bonnier, Y. Leroyer, and C. Meyers, Phys. Rev. B **40**, 8961 (1989).
[54] R. P. Cody and G. K. Smith, *Applied Statistics and the SAS Programing Language* 4th ed. (Prentice Hall, Princeton, NJ, 1997), p. 115.
[55] E. Domany, S. Alexander, D. Bensimon, and L. P. Kadanoff, Phys. Rev. B **28**, 3110 (1983).
[56] G. Pruessner, D. Loison, and K. D. Schotte, Phys. Rev. B **64**, 134414 (2001).
[57] M. El-Hilo, K. O'Grady, and R. W. Chantrell, J. Magn. Magn. Mater. **120**, 244 (1993).
[58] O. Penrose, J. Stat. Phys. **45**, 69 (1986).